INTERFACE

rsif.royalsocietypublishing.org

Research

Cite this article: Pasquini L *et al*. 2015 Isotropic microscale mechanical properties of coral skeletons. *J. R. Soc. Interface* **12**: 20150168.
http://dx.doi.org/10.1098/rsif.2015.0168

Received: 25 February 2015
Accepted: 18 March 2015

Subject Areas:
biomaterials

Keywords:
corals, mechanical properties, microstructure, biomaterial

Authors for correspondence:
Luca Pasquini
e-mail: luca.pasquini@unibo.it
Giuseppe Falini
e-mail: giuseppe.falini@unibo.it

Electronic supplementary material is available at http://dx.doi.org/10.1098/rsif.2015.0168 or via http://rsif.royalsocietypublishing.org.

THE ROYAL SOCIETY PUBLISHING

Isotropic microscale mechanical properties of coral skeletons

Luca Pasquini[1], Alan Molinari[1], Paola Fantazzini[1], Yannicke Dauphen[2], Jean-Pierre Cuif[2], Oren Levy[3], Zvy Dubinsky[3], Erik Caroselli[4], Fiorella Prada[4], Stefano Goffredo[4], Matteo Di Giosia[5], Michela Reggi[5] and Giuseppe Falini[5]

[1]Department of Physics and Astronomy, Alma Mater Studiorum-Università di Bologna, viale Berti Pichat 6/2, 40127 Bologna, Italy
[2]Université Paris-Sud, Orsay, Bat. 504, UMR IDES, 91405 Orsay, France
[3]The Mina and Everard Goodman Faculty of Life Sciences, Bar-Ilan University, Ramat-Gan 52900, Israel
[4]Department of Biological, Geological and Environmental Sciences, Section of Biology, Alma Mater Studiorum-Università di Bologna, via Selmi 3, 40126 Bologna, Italy
[5]Department of Chemistry 'Giacomo Ciamician', Alma Mater Studiorum-Università di Bologna, via Selmi 2, 40126 Bologna, Italy

Scleractinian corals are a major source of biogenic calcium carbonate, yet the relationship between their skeletal microstructure and mechanical properties has been scarcely studied. In this work, the skeletons of two coral species: solitary *Balanophyllia europaea* and colonial *Stylophora pistillata*, were investigated by nanoindentation. The hardness H_{IT} and Young's modulus E_{IT} were determined from the analysis of several load–depth data on two perpendicular sections of the skeletons: longitudinal (parallel to the main growth axis) and transverse. Within the experimental and statistical uncertainty, the average values of the mechanical parameters are independent on the section's orientation. The hydration state of the skeletons did not affect the mechanical properties. The measured values, E_{IT} in the 76–77 GPa range, and H_{IT} in the 4.9–5.1 GPa range, are close to the ones expected for polycrystalline pure aragonite. Notably, a small difference in H_{IT} is observed between the species. Different from corals, single-crystal aragonite and the nacreous layer of the seashell *Atrina rigida* exhibit clearly orientation-dependent mechanical properties. The homogeneous and isotropic mechanical behaviour of the coral skeletons at the microscale is correlated with the microstructure, observed by electron microscopy and atomic force microscopy, and with the X-ray diffraction patterns of the longitudinal and transverse sections.

1. Introduction

Scleractinian corals represent a major source of biogenic calcium carbonate [1,2] and are among the fastest marine mineralizing organisms [3]. Their skeleton is a composite structure with both inorganic (aragonite) and organic components [4]. The content of organic components and structural water ranges between 1 and 3 wt%, whereas non-structural water represents a minor component being present in amounts lower than 0.5 wt% [5]. One of the most important roles of coral skeletons is the building of the structure on which the soft tissue can grow and be protected. The skeletal structure of the corals also make the framework of the reef, which has an important ecological, economical and social relevance [6]. A detailed description of corals' skeletal texture and morphogenesis is reported in several reviews (e.g. [2,7] and references therein). The basic building blocks of all parts of all coral skeletons are the sclerodermites, consisting of fine aragonite crystals or fibres arranged in three-dimensional fans around a centre of calcification. The aragonite fibres, approximately 0.05 − 4 μm in diameter, are elongated along the crystallographic *c*-axis. They grow as spherulites, grouped into bundles termed fascicles [8]. The diameters and morphologies of individual aragonite fibres are taxonomically distinct. A number of sclerodermites growing upwards together develop into

a vertical spine called a trabecula. Groups of trabeculae, united with or without intervening spaces (or pores) form the septa, the primary structures of the coral skeleton. In the recent years, the merging of data from several investigations has revealed that the actual building unit of the skeleton is a mineralizing growth layer a few micrometres thick, synchronically produced for a given septum zone [9,10].

Because the skeleton of corals has a peculiar architecture, is not homogeneous in the texture and shows a hierarchical organization [9], the study of its mechanical properties at the nano-microscale can overcome the limitation presented by the sample structural heterogeneity at the macroscale.

The understanding of the mechanical properties of the skeleton at the nano-microscale are important to study the survival of corals. Indeed, although they do not rely on their skeletons in exactly the same way as many other organisms do, skeletal strength can limit viable colony or branch size or influence growth form. The mechanical properties can determine the range of hydraulic conditions a colony can withstand, or can influence the selection of suitable habitats. Knowledge of the skeletal mechanics of modern coral, and its relation to microstructure, has also great potential for interpreting the palaeoecology of fossil corals. Indeed, measurement of the compressive strength and elastic modulus of the skeletal material of three common Caribbean corals suggested that the mechanical properties of coral skeletons are an important factor in the adaptive repertoire of these animals [11].

Coral mechanical properties are also important from the applicative point of view, because scleractinian corals were used as bone graft substitutes [12] having good biocompatibility and biodegradation, and mechanics similar to those of human cancellous bone.

Nanoindentation techniques have recently been adapted for the study of biological materials and are a powerful tool for study of the mechanical properties at the nano-microscale. The analysis of the platelets on the nacreous layer of the red abalone shell showed that the deformability of the aragonite platelets together with the crack deflection, aragonite platelet slip and organic adhesive interlayer contribute to the nacre's fracture toughness [13]. Sea urchin spines from *Heterocentrotus mammillatus*, *Phyllacanthus imperialis* and *Prionocidaris baculosa* showed a strong dependence of the indentation modulus, but not the indentation hardness, on the local porosity. This was attributed to the network type of porosity [14]. The hardness and modulus of biogenic calcite from the prismatic layer of the mollusc *Atrina rigida* was compared with a pure geological calcite, Iceland spar. On the (001) face, biogenic calcite was found to be 50–70% harder than geologic calcite. The higher hardness and increased anisotropy of biogenic calcite was accounted for by hardening mechanisms based on hindered dislocation motion rather than on crack deflection [15]. The mechanical properties of the nacreous layer of five different seashells were investigated by nanoindentation and three-point-bending tests: it was found that the aspect ratio of the mineral phase in all seashells is close to the optimal value for strength as predicted by theory [16]. The multiscale mechanical properties of nacre, from the single aragonite platelet to the composite brick-and-mortar structure, were studied with great care using a combination of spherical and sharp nanoindentation tests. The elastic properties of the intracrystalline organic phase and its role in the deformation of the aragonite platelet were elucidated [17].

The compressive strength of *Acropora* sp., *Goniopora* sp. and *Porites* sp. on randomly oriented samples ranged between 2 and 12 MPa [18] similar to that of wet cancellous bone, which ranges from 1 to 12 MPa [19]. Different from the case of bone, the compressive strength of corals was not affected by their hydration state [10].

Here, we report a nanoindentation investigation on the skeletons of solitary *Balanophyllia europaea* and colonial *Stylophora pistillata* scleractinian corals. The rationale for the selection of these two corals species is that they do not live in the same type of habitat (Mediterranean versus tropical) and thus are subjected to completely different environmental conditions that could affect the mechanical properties at the microstructure level. In addition, *S. pistillata* is colonial, and thus builds branched structures, whereas *B. europaea* is solitary and grows as a unique cap. Moreover, they are both symbiotic with unicellular algae called zooxanthellae, which provide them an additional energetic approach to photosynthesis. The aim of this study is to determine whether an orientation-dependence of the mechanical properties arises as a consequence of the diverse growing environment and growth form, discussing the ecological and applicative implications.

2. Material and methods

2.1. Specimen preparation

The coral samples of *B. europaea* from Palinuro (Italian coast, Nord-Western Mediterranean Sea) were randomly collected by scuba diving at 6 m depth on 25 February 2012. Samples of *S. pistillata* were collected by scuba diving at a depth of 10 m in the Gulf of Eilat (Red Sea) during May 2012. These samples were collected under permission. For each species, three skeletons were investigated using different techniques as described later on. In order to obtain clean coral skeletons, the coral tissue was first totally removed by immersing the samples in a solution of 10% commercial bleach for 3 days. Corals were then dried for 4 days at a maximum temperature of 50°C to avoid any possible transition in the skeletal carbonate phases [20]. The samples were inspected under a binocular microscope to mechanically remove possible fragments of sediment, rocks and encrusting organisms with the aid of a scalpel. In the case of solitary *B. europaea*, the skeleton coincides with a single individual, whereas for *S. pistillata*, it corresponds to one branch of a ramified coral colonized by many small polyps (figure 1). The main axis of the skeleton can be identified in the oral–aboral axis for *B. europaea* and in the branch growth direction for *S. pistillata*.

As reference aragonite-based materials for comparison of corals mechanical properties, we examined the nacreous layer of the seashell *A. rigida* (named simply nacre from here on) and geogenic aragonite single crystals. The *A. rigida* shell was kindly provided by the Mostra Mondiale di Malacologia (Cupra Marittima, Italy). The geogenic aragonite (from Morocco) was bought in a mineral market in Bologna, Italy.

For X-ray diffraction (XRD), atomic force microscopy (AFM) and nanoindentation measurements, two perpendicular sections, longitudinal and transverse, were prepared by embedding, cutting and polishing using standard metallographic techniques (figure 1). The skeletons were first embedded in a highly impregnating epoxy resin under vacuum conditions (10^{-1} mbar) to guarantee the filling of open pores and channels. The purpose of embedding is twofold: to preserve the skeletal integrity during subsequent cutting/polishing, and to obtain a continuous flat section after cutting, as needed by nanoindentation tests. After a hardening period of 24 h, the samples were cut with a rotating diamond blade. To obtain the longitudinal section, a cutting

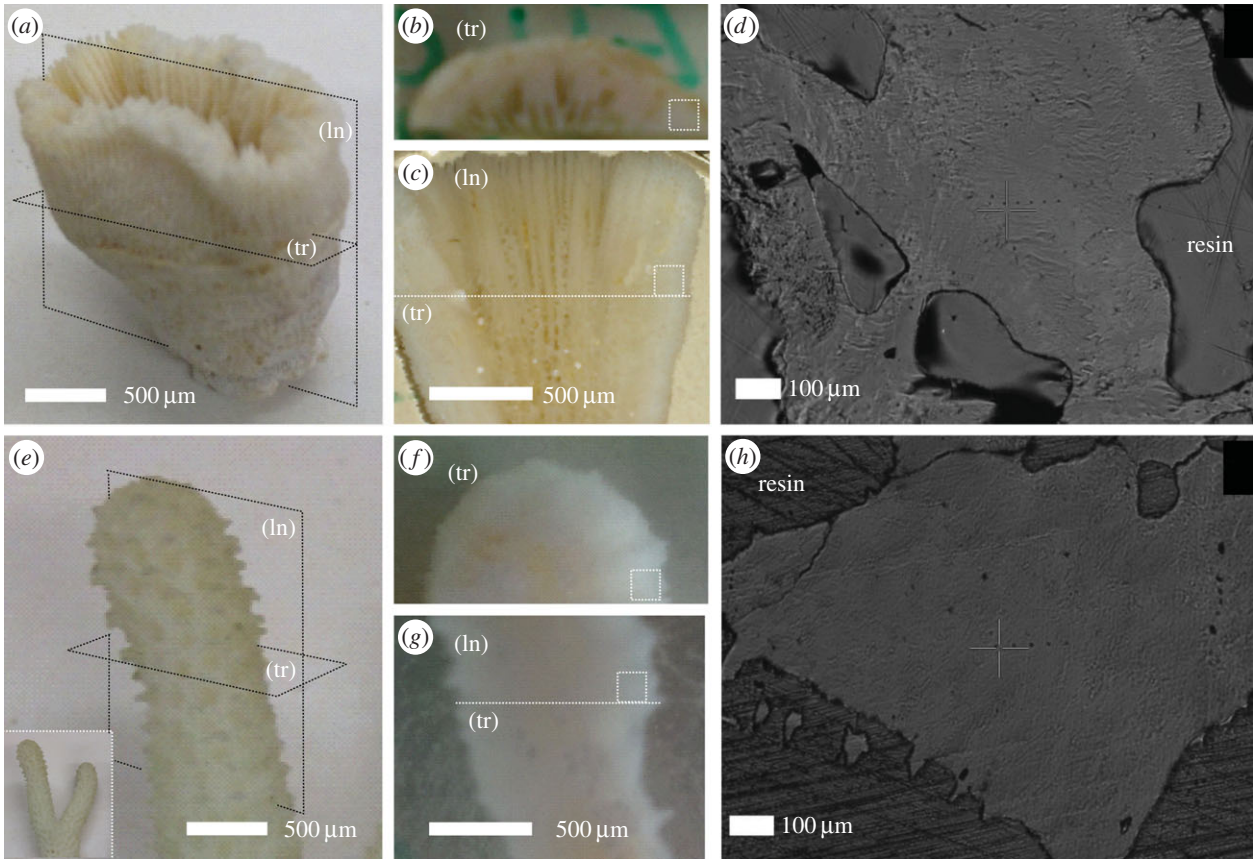

Figure 1. Camera pictures of the intact skeletons of *B. europaea* (*a*) and *S. pistillata* (*e*) corals, showing longitudinal (ln) and transverse (tr) cutting planes with respect to the main growth axis. The polished sections obtained from these cuts are displayed in (*b,c*) for *B. europaea* and (*f,g*) for *S. pistillata*. The dotted squares in these pictures indicate the regions were nanoindentation tests were carried out, while the dotted line in (*c,g*) indicates the direction of cutting to obtain the transverse section. The corresponding videomicroscope images, recorded *in situ* in the nanoindenter, are reported in (*g*) for *B. europaea* and (*h*) for *S. pistillata* A series of aligned indentations is visible in both images to the right of the cross-shaped marker. (Online version in colour.)

plane was selected which contains the skeleton main axis. Conversely, for the transverse section, the cutting plane was perpendicular to the main axis. The camera pictures in figure 1*a–c* (*B. europaea*) and figure 1*e–g* (*S. pistillata*) illustrate the relation between the two sections and the intact skeleton. The sections were polished first with silicon carbide sandpaper of two decreasing grit sizes (P600 and P1200) and then by alumina (Al_2O_3) colloidal suspensions of three decreasing grain sizes: 3–1, 0.5–0.3 and 0.05 µm. Figure 1 displays the relevant optical images of the polished sections.

In addition, for reference aragonite-based materials, two differently oriented sections were examined. Nacre was cut, after embedding in resin, parallel and perpendicular to the cross section of the layer, and polished using the same procedure of corals. In the case of geogenic aragonite, the (001) and (122) surfaces were prepared for subsequent analyses by embedding two single crystals in different orientations, without any polishing.

2.2. Nanoindentation

The mechanical properties were measured with a TTX-NHT nanoindentation tester (CSM Instruments), equipped with a Berkovich diamond indenter (tip opening angle = 142.3°), an optical videomicroscope and a motorized translation table. Ten indentations tests, with a minimum distance of 30 µm between two tests, were carried out both on the longitudinal and on the transverse section of three skeletons per coral species. Care was also taken to keep a minimum distance of 50 µm from the coral edges and from microscale pores visible on the surface. This is important in order to avoid artefacts owing to the presence of elastic discontinuities in proximity of the indentation area. If the indentation areas on the two perpendicular sections are properly selected, this procedure amounts to indenting a small volume (less than 1 mm^3) of the original skeleton along two perpendicular directions. Figure 1 also displays videomicroscope images of typical indentation zones for *B. europaea* (*d*) and *S. pistillata* (*h*). A series of aligned indentations is visible to the right of the cross-shaped marker.

All measurements were done on dry samples. In order to check whether the hydration state influences the mechanical properties, measurements in wet state were also performed after soaking the polished sections in an aragonite-saturated solution for 16 h.

The measurements were conducted in load-control mode using the following settings: maximum load = 50 mN, loading/unloading rate = 100 mN min^{-1}, holding period at maximum load = 10 s. In addition, for each section, one indentation was performed in dynamic sinus mode, in which an oscillation at 5 Hz and 10% amplitude was superimposed to the rising load. The instrumented Young's modulus E_{IT} and hardness H_{IT} were determined by the Oliver & Pharr (O–P) method [21]: H_{IT} is given by the ratio between the maximum applied load and the corresponding projected contact area, whereas E_{IT} is derived from the initial slope of the load–displacement curve during unloading. The dynamic analysis of sinus-mode measurements permits determination of H_{IT} and E_{IT} as a function of the penetration depth.

2.3. X-ray diffraction, scanning electron microscopy, thermogravimetrical analyses and atomic force microscopy measurements

XRD profiles of each section were collected using an X-Celerator powder diffractometer (PANalytical), using Cu-Kα radiation (λ = 1.540 Å). For the sake of comparison, the XRD profile of aragonite powders was collected under the same conditions.

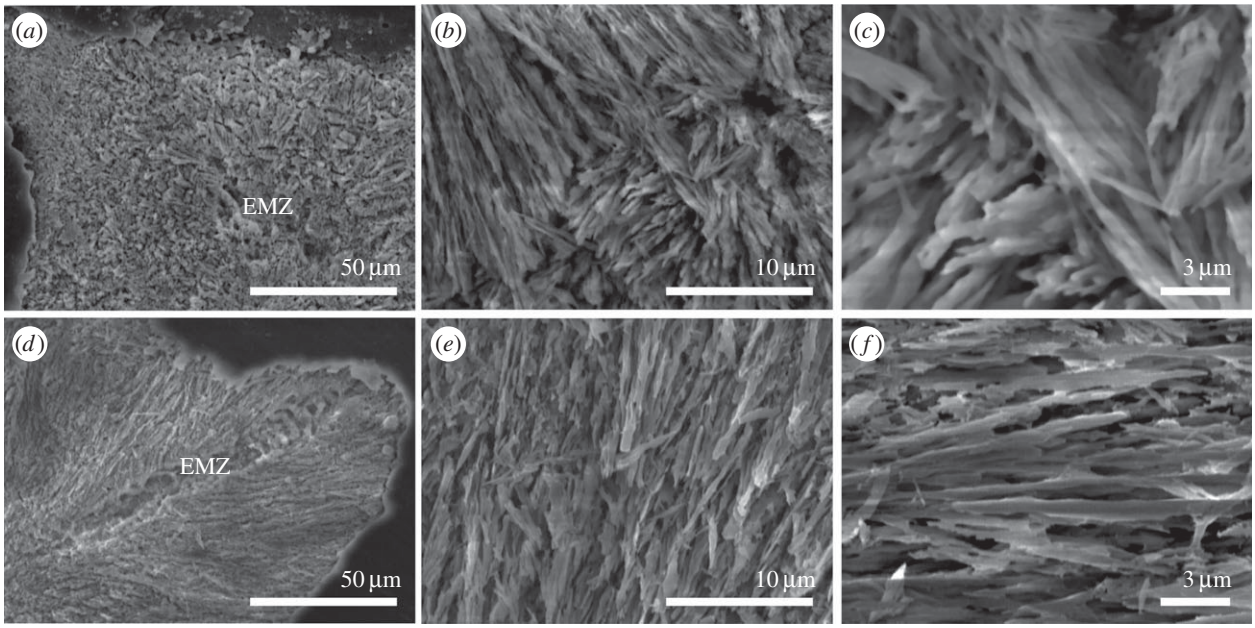

Figure 2. Scanning electron microscope pictures of a cross section of the growing tip of the coral skeletons of *B. europaea* (*a–c*) and S. *pistillata* (*d–f*). EMZ indicates the early mineralization zone structural motif from which the growth of the radiating aragonite fibres starts. Panels (*b,c*) and (*e,f*) show pictures of the skeleton fibre region of *B. europaea* and *S. pistillata*, respectively, at increasing magnifications.

Scanning electron microscope (SEM) observations were conducted using a Phenom^{TM} microscope (5 kV, FEI) for uncoated samples and a Hitachi FEG 6400 microscope (20 kV) for samples coated with gold. Images of residual imprints were recorded *in situ* after the measurements with the videomicroscope of the nanoindentation tester and using the Phenom^{TM} microscope. For AFM observations, the sections were further polished using diamond paste and cleaned with Milli-Q water (resistivity 18.2 MΩ cm at 25°C; filtered through a 0.22 µm membrane). They were observed using a Veeco AFM dimension 3100 Nanoscope III. The probe consists of a cantilever with an integrated silicon nitride tip. Samples were imaged at room temperature and in air using taping mode phase contrast imaging.

Thermogravimetrical analyses (TGA) were carried out on ground samples using Instruments SDT 2960 at a heating rate of 10°C min^{-1} in a nitrogen atmosphere over a temperature range from 30 to 600°C. Sample weights were 3–5 mg, and the nitrogen flow rate was 100 ml min^{-1}. The content of non-structural water and of organic matrix plus structural water [5] was evaluated from the weight lost between 90°C and 150°C and between 250°C and 350°C, respectively. Six measurements (two for each skeleton) were carried out for each species.

3. Results

3.1. Microstructure of coral skeletons

The SEM images in figure 2 display cross sections of fractured coral skeletons in the region close to the growing tip. The architecture of the microstructure is clearly visible in the two constituting units: the early mineralization zone, EMZ (indicated), and the aragonitic fibres. The location of the EMZs is random in *B. europaea*, whereas EMZs are aligned along the growing direction of the tip in *S. pistillata*. The aragonitic fibres do not show any preferential direction of growth in both species. The length scale of their rhythmic growth is shorter in *B. europaea* (less than 10 µm) than in *S. pistillata* (more than 20 µm), whereas their thickness does not exhibit differences between the two species (300–500 nm).

Figure 3 reports AFM images and X-ray diffraction profiles of the longitudinal and transverse skeletal sections. The relative intensities of the Bragg reflections display the same pattern for all profiles. The similarity to the diffraction pattern of polycrystalline aragonite (JCPDS 41-1475) suggests the absence of preferential orientations of aragonite crystallites. The width of the reflections does not change between the two species, indicating similar average dimensions of the crystalline domains. This observation is also confirmed by the AFM images (figure 3), which enabled the spheroid building units of the aragonitic fibres to be observed. The images show a similar shape distribution and organization of the aragonitic spheroids independently on the direction of observation in both coral species. The content of the organic matrix in *B. europaea* and *S. pistillata* was of 2.2 ± 0.1 wt% and 1.4 ± 0.1 wt%, respectively, from TGA.

3.2. Young's modulus and hardness of coral skeletons

Figures 4 and 5 show the load–depth nanoindentation curves measured on a single dry skeleton of the two coral species. In figures 4 and 5*a,b*, it is possible to note that a relatively small variability exists between tests carried out on the same section. The resulting average curves, obtained for the two sections separately, are very close to each other: as shown in figures 4 and 5*c*, the discrepancy between them is, indeed, lower than the typical spread between the curves in a single section. This consideration applies to both coral species and to all examined skeletons.

The E_{IT} and H_{IT} values derived from the quantitative O–P analysis of load–depth curves are summarized in table 1, where the data pertaining to each coral species represent an average over the three examined skeletons. The results of a mixed-factorial analysis of variance applied to the whole dataset are reported in the supplementary material, tables S1 (E_{IT}) and S2 (H_{IT}). Species and orientation were taken as the between subjects factor and within subjects factor, respectively. This statistical analysis of skeletal mechanical properties clearly

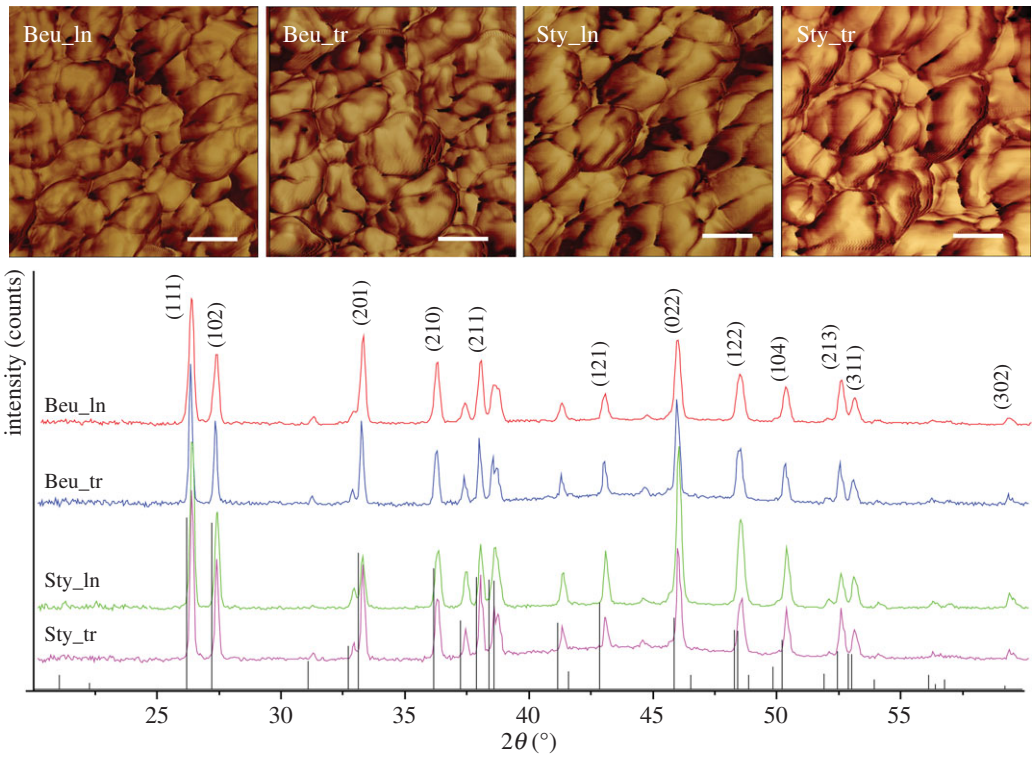

Figure 3. *Top*: AFM images of cross sections of *B. europaea* (Beu) and *S. pistillata* (Sty) coral skeletons embedded in resin and cut along the longitudinal (ln) and transverse (tr) direction with respect to the main growth axis. Z range 180°. Scale bar, 50 nm. *Bottom:* corresponding XRD diffraction profiles, the main diffraction peaks are marked with the Miller indices (JCPDS 41-1475). The images and the diffraction patterns are representative of all the samples analysed. (Online version in colour.)

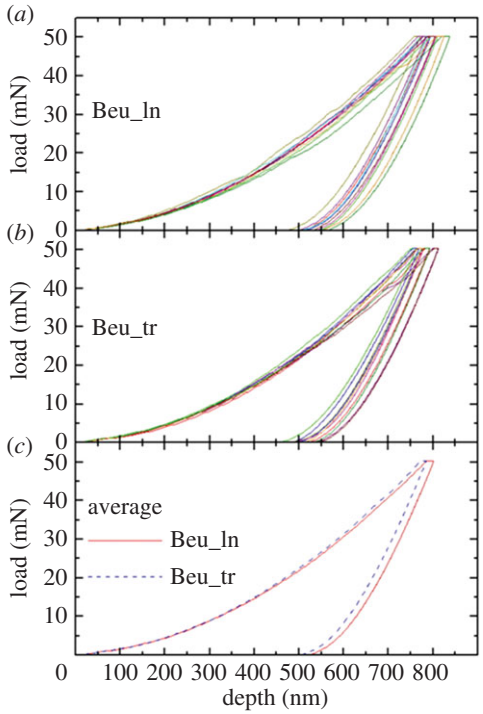

Figure 4. Load–depth nanoindentation measurements on a single skeleton of *B. europaea* (Beu): a sequence of 10 indentations was carried out on (*a*) longitudinal (ln) and (*b*) transverse (tr) sections. In (*c*), the resulting average curves for the two sections are compared. (Online version in colour.)

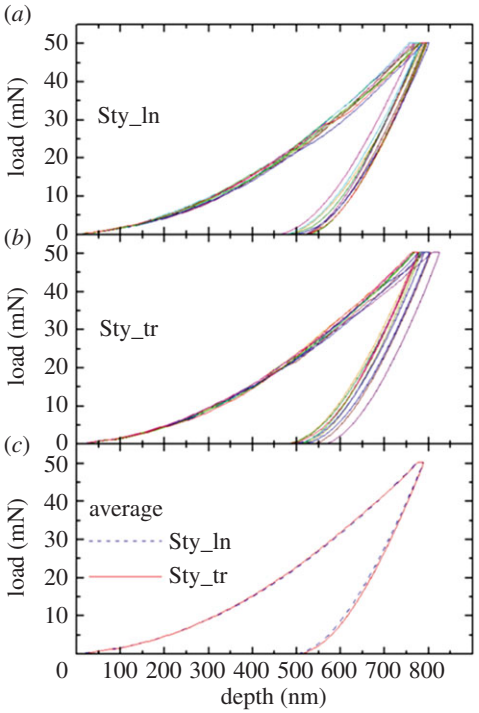

Figure 5. Load–depth nanoindentation measurements on a single skeleton of *S. pistillata* (Sty): a sequence of 10 indentations was carried out on (*a*) longitudinal (ln) and (*b*) transverse (tr) sections. In (*c*), the resulting average curves for the two sections are compared. (Online version in colour.)

shows that (i) there is no significant difference between the longitudinal and transverse sections (this is true for both species); (ii) in the case of Young's modulus E_{IT}, there is no significant difference between the two species; (iii) in the case of hardness H_{IT}, there is a small yet statistically significant difference between the two species, with *S. pistillata* being about 3% harder than *B. europaea*.

The dynamic sinus measurements, reported in electronic supplementary material in figures S2–S3 for the longitudinal sections of the two species, demonstrate that the corals'

Table 1. Average values of Young's modulus E_{IT} and Hardness H_{IT} obtained from nanoindentation measurements on differently oriented sections of the two coral species, *A. rigida* (nacreous layer) and geogenic single-crystal aragonite. The number of individual measurements per section is 30 for the two coral species (10 × 3 skeletons per species), 10 for *A. rigida* and 10 for geogenic aragonite. The standard error is given in parenthesis, in units of the last significant digit.

material	section orientation	E_{IT} (GPa)	H_{IT} (GPa)
B. europaea	longitudinal	77.0 (11)	4.87 (3)
	transverse	76.3 (5)	4.97 (6)
S. pistillata	longitudinal	76.6 (11)	5.04 (3)
	transverse	76.0 (5)	5.10 (6)
A. rigida (nacreous layer)	S1[a]	55.0 (3)	3.49 (5)
	S2[a]	67.4 (4)	3.25 (4)
aragonite (single crystal)	(001)	100.8 (8)	7.30 (10)
	(122)	82.7 (9)	4.15 (6)

[a]S1 and S2 indicate surfaces perpendicular and parallel, respectively, to the nacreous layer cross section.

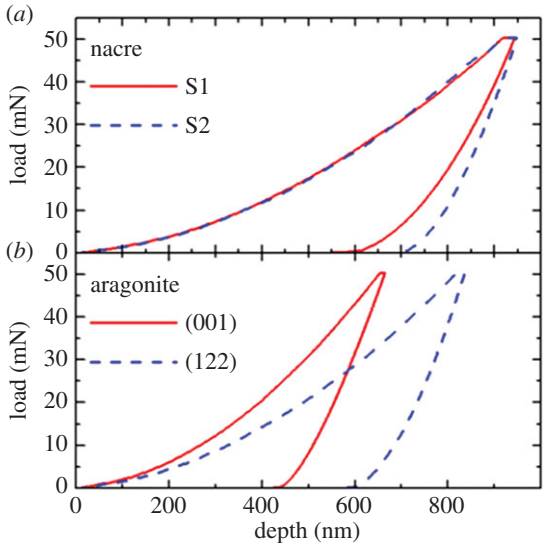

Figure 6. Load–depth nanoindentation measurements on two different sections of (*a*) nacreous layer of *A. rigida* and (*b*) single-crystal aragonite. The displayed curves represent an average over 10 indentations. S1 and S2 indicate surfaces perpendicular and parallel, respectively, to the nacreous layer cross section. (Online version in colour.)

mechanical properties do not depend significantly on the indentation depth in the probed range. The same conclusion applies to the transverse sections of the two corals.

Finally, we note that the nanoindentation curves as well as the mechanical parameters E_{IT} and H_{IT} measured on the wet sections are identical to the ones obtained from the dry sections within statistical uncertainties (electronic supplementary material, figure S1).

3.3. Comparison with other aragonite-based materials

At variance with coral skeletons, in the case of nacre a significant difference between longitudinal and transverse sections is observed in the unloading average curves (figure 6*a*), revealing a clear anisotropy of the mechanical properties. The anisotropy becomes even more evident in single-crystal aragonite (figure 6*b*), where the average nanoindentation curves for the (001) and (122) sections exhibit a remarkable difference both in the residual depth and in the unloading slope. According to the O–P analysis reported in table 1, nacre exhibits a strong E_{IT} anisotropy and a weak H_{IT} anisotropy, whereas for single-crystal aragonite, both E_{IT} and H_{IT} strongly depend on the indentation direction. The corals' mechanical parameters, $E_{IT} \sim 76–77$ GPa and $H_{IT} \sim 4.9–5.1$ GPa, are higher than those of the nacreous layer in *A. rigida*, and lower than those of the stiff and hard (001) direction of single-crystal aragonite. They appear close to the values determined for the compliant and soft (122) direction.

3.4. Residual indents and crack generation

Typical optical images of the residual indents on the corals' skeletons, recorded *in situ* right after the measurements, are displayed in electronic supplementary material, figure S4. The side of the residual indentation triangle is ≈ 5 µm. In some cases, the surface around the indent edges appears very flat (electronic supplementary material, figure S4*a*,*c*), whereas in others, a disturbance of the surface is observed (electronic supplementary material, figure S4*b*,*d*). Higher magnification SEM images of these residual indents clearly show the occurrence of the pile-up of material as a result of the plastic deformation. An example is reported in figure 7, where the generation of a radial crack is also detected in the proximity of the indent's bottom corner.

The occurrence of pile-up and microcracks was examined in more detail for *B. europaea* by performing further groups of 10 indentations with maximum loads of 5 and 500 mN. At 5 mN maximum load, we hardly observed any pile-up formation or microcrack generation. At 500 mN maximum load, crack generation was almost ubiquitous, making it possible to measure the length of the developed radial cracks under the videomicroscope (electronic supplementary material, figure S5). The length of the crack enables the determination of another interesting mechanical property, i.e. the fracture toughness K_c, according to a described procedure [22 and references therein]. Even though a precise estimation of K_c is difficult, owing to the variability of crack length, we can assert that also the fracture toughness of the corals' skeletons is independent on the indentation direction: $K_c = 0.6 \pm 0.1$ MPa $m^{1/2}$ and $K_c = 0.5 \pm 0.1$ MPa $m^{1/2}$ for the longitudinal and transverse sections, respectively. Conversely, no microcrack generation was observed in nacre even at the highest load of 500 mN, indicating a higher fracture toughness of nacre with respect to the corals' skeletons.

4. Discussion

4.1. Anisotropic mechanical properties of single-crystal aragonite

The measurements on single-crystal aragonite highlight that its mechanical properties, both in the elastic and plastic deformation regimes, are highly anisotropic, as already reported on the basis of microhardness measurements [23] and nanoindentation tests [24]. An orthorhombic crystal, like aragonite, has nine independent elastic constants C_{ij} [25], which fully determine its stress–strain relationships. The

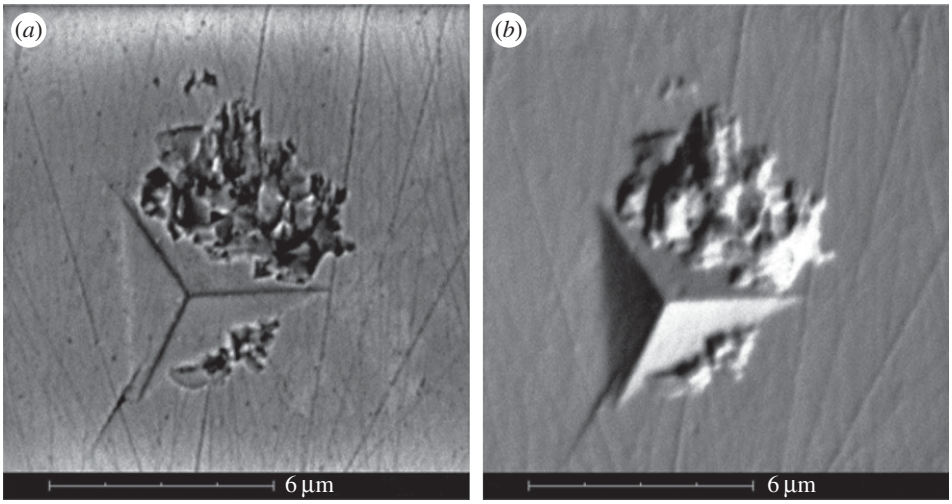

Figure 7. SEM images of a residual indent on the transverse section of *B. europaea*, taken in 'backscattered' (*a*) and 'backscattered shadow' (*b*) modes. The images show both the generation of a radial crack starting in proximity of the bottom corner, and the pile-up of material around the indent. The thin straight lines are residuals of the polishing procedure.

Young's modulus along each lattice direction results from the combination of a specific C_{ij} subset. Therefore, if the C_{ij} exhibit significant anisotropy, as reported for aragonite [26] ($C_{11} = 171.1 \pm 1.0$ GPa and $C_{33} = 98.4 \pm 1.2$ GPa), so will the Young's modulus. In particular, the Young's modulus along the [001] direction (*c*-axis), which can be determined from the nanoindentation tests perpendicular to the {001} planes, is given by the simple relation $E[001] = C_{33}$. Our measured value $E[001] = 100.8 \pm 0.8$ (table 1, result on section (001)) is thus in excellent agreement with the elastic constants measured by Brillouin spectroscopy [26] and with previous nanoindentation measurements (102.8 ± 2.4 [24]). For polycrystalline aragonite, the aggregate Young's modulus was calculated as $E = 91.5$ GPa in reference [26] using the Voigt–Reuss–Hill averaging scheme. Other experiments and first principles calculations, however, report a slightly reduced bulk modulus than reference [26], resulting in a lower $E =$ 86 GPa [27]. Thus, the Young's modulus value for pure, polycrystalline aragonite shall be expected in this range, i.e. approximately from 85 to 90% of $E[001]$.

The plastic deformation of aragonite appears even more anisotropic. In reference [24], the values $H_{IT} = 6.2 \pm 0.3$ GPa and $H_{IT} = 4.4 \pm 0.4$ GPa were reported for nanoindentation tests perpendicular to the planes (001) and $(\bar{1}30)$. The microscopic origin of this behaviour is the existence of preferential slip systems, such as the {110}<001> family [24]. The pile-up effect around the indentations was described correctly by a crystal plasticity model, which takes into account all the slip systems [24]. Our values (table 1) are in good agreement with reference [24] and confirm the strong anisotropy of the nanoindentation hardness. The slightly higher hardness measured here for the section (001) could be attributed to a higher concentration of impurities in our geogenic aragonite, acting as pinning centres for dislocations.

4.2. Anisotropic mechanical properties of nacre

The mechanical properties of nacre and their relation to the material's microstructure are an intensively studied subject as mentioned in the introduction [13,15–17]. Our motivation for measuring nacre was to achieve a direct comparison, i.e. using the same equipment and protocol, with the mechanical properties of coral skeletons. Fleischli *et al.* have shown that both hardness and Young's modulus strongly depend on the scale of nacre's well-known brick-and-mortar architecture, especially on the thickness of the aragonite platelets. In the seashells with thick platelets, in particular *Trochus maculatus* and *Haliotis rufescens*, the values of E_{IT} and H_{IT} are close to pure aragonite [16]. Conversely, in the seashells characterized by thin platelets, such as those of *Pteria penguin*, a Young's modulus as low as 60 ± 8 GPa and a hardness of 3.7 ± 1.0 GPa were measured [16]. Our values for the nacreous layer of *A. rigida* (table 1) fall within this range [16]. Such reduced values are generally attributed to the high weight fraction, around 6 wt%, of organic matrix (the mortar), which is orders of magnitude softer and more compliant than aragonite [16].

The significant Young's modulus anisotropy in nacre, highlighted by our measurements, originates with the previously discussed anisotropy of the aragonite platelets (the bricks), which are aligned preferentially along one crystallographic direction within the nacreous layer.

The absence of radial cracks after 500 mN indentation witnesses the high fracture toughness of nacre. Li *et al.* showed that this behaviour arises from the ductility of nanograined aragonite platelets, coupled with crack deflection, platelet slip and organic adhesive interlayer. The elevated content of the organic matrix plays a decisive role in nacre's fracture resistance [13].

4.3. Isotropic mechanical properties of coral skeletons

The statistical analysis of nanoindentation data (table 1 and electronic supplementary material, tables S1 and S2) proves that coral skeletons, in contradistinction to nacre, exhibit isotropic mechanical behaviour at the microscale both in the elastic and plastic regimes, despite the remarkable mechanical anisotropy of aragonite. In addition, relatively small fluctuations, in the range of about 3% for E_{IT} and 6% for H_{IT}, were detected within the same section (figures 4 and 5), indicating a homogeneous mechanical response on a spatial scale larger than the typical indentation volume.

These features can be explained by the spatial arrangement of aragonite crystals, as highlighted by SEM and AFM observations (figures 2 and 3) and XRD profiles (figure 3). In fact, SEM shows that the aragonite fibrous crystals are about

200–400 nm thick, i.e. much thinner than the typical indentation size (5–10 µm), and are oriented along different directions in a fan-like arrangement: each indentation, therefore, represents an average over many differently oriented crystals, resulting in a homogeneous response across a section. The absence of preferential orientation of the aragonite crystals suggested by XRD (figure 3) explains why the mechanical parameters are the same in the two perpendicular sections. Finally, the AFM observations of the fibrous crystals (figure 3) agree with the above data showing an isotropic distribution of the spheroidal units making the fibrous crystals. In summary, the architectural arrangement of its basic building units confers to the skeleton a nearly perfect isotropic microscale mechanical behaviour in the elastic and plastic deformation regime. This consideration probably also extends to the fracture behaviour, even though further experiments are needed to better assess this point.

4.4. Effects of porosity and organic matrix on skeletal mechanical properties

The small fluctuations observed within the same section may arise from local variations, from one indentation site to another, of one or more of the following items

(1) Average orientation of aragonite crystals: although XRD reveals no preferential orientation over the whole section, it is not possible to rule out small changes on the micrometre scale.
(2) Pore content: as shown by Presser *et al.* [14], local porosity influences the mechanical properties determined by nanoindentation, in particular lowering Young's modulus with respect to a fully dense material. Using time-domain nuclear magnetic relaxometry, we have shown that coral skeletons contain pores with sizes ranging from about 10 µm down to few tens of nanometres [28]. Such pores may either be too small to be detected under the videomicroscope or be hidden beneath the surface, and their varying concentration could contribute to the observed fluctuations.
(3) Abundance of the organic matrix [7,29]: Stempflé *et al.* have shown that both the intercrystalline and intracrystalline organic matrix, characterized by low Young's modulus (6.3 and 3.8 GPa, respectively), play an important role in the elastic and plastic deformation of nacre's aragonite platelets [17]. As already recalled, it is expected that regions richer in organic matrix display lower Young's modulus and hardness.

The influence of porosity and organic matrix on the mechanical properties can also explain the lower Young's modulus of coral skeletons with respect to polycrystalline aragonite. Similarly, the difference in hardness between the two coral species may reflect a lower content of organic matrix and possibly porosity in *S. pistillata* with respect to *B. europaea*. Indeed, TGA detects a lower content of organic matrix in *S. pistillata* (1.4 ± 0.1 wt%) than in *B. europaea* (2.2 ± 0.1 wt%). However, the difference in hardness is very small (only 3%, while fluctuations up to 100% between different seashell species have been reported [16]), making it difficult to ascribe it to a specific mechanism. The comparison between microscale mechanical properties of several coral species having diverse organic matrix content and porosity may be the subject of future studies.

4.5. Implications of isotropic mechanical properties of coral skeletons

These data have implications regarding the corals' ecology and the application of coral skeletons as bone graft materials. Indeed, the mechanical isotropy offers corals the advantage to grow, irrespective of the direction, letting the construction of their complex architectures be driven by other vital parameters, such as the intensity and directionality of the underwater light field [30], the current velocity [31] and the gravity [32]. The coral mechanical isotropy is also relevant to the use of coral as cancellous bone grafting. Indeed, cancellous bone is a mechanically anisotropic biomineral [33–35], like nacre [36], with a wide range of elasticity depending on the source [16,37]. Thus, an isotropic biocompatible and biodegradable material could be applied also to cancellous bones where a diverse anisotropy is present.

5. Conclusion

The Young's modulus and hardness measured on the coral skeletons of *B. europaea* and *S. pistillata* are in the ranges 76–77 GPa and 4.9–5.1 GPa, respectively. The statistical analysis does not reveal a significant difference between skeletal sections having different orientations with respect to the main growth axis of the coral. The Young's modulus is the same for the two coral species, whereas hardness is approximately 3% lower in *B. europaea*. The mechanical properties are also rather constant over different indentation sites, typically separated by few tens of micrometres within one section. SEM, AFM and XRD show that this behaviour originates from the random orientation of aragonite fibres, and their forming spheroid particles, which are much thinner than the indentation size. Despite the significant anisotropy of the building units (aragonite crystals), the coral skeletal material is thus homogeneous and isotropic as concerns the mechanical properties at the microscale. Orientation dependence of the mechanical properties of the entire skeleton, if present, should therefore be ascribed to its anisotropic shape on a larger (i.e. mm to cm) scale. The slightly lower Young's modulus (by about 10%) with respect to pure polycrystalline aragonite can be ascribed to the presence of microporosity and soft organic matrix in the coral skeletons. In comparison, the widely studied nacre material exhibits a clear anisotropy of Young's modulus and a significant variation among different seashell species. Both features can be attributed to the highly organized 'brick-and-mortar' architecture of nacre, the features of which (shape and thickness of the aragonite platelet, content of the organic matrix) vary strongly among different seashells. These observations have implications in corals' ecology and in the use of coral skeletons as bone graft substitutes.

Acknowledgements. G.F. thanks the Consorzio Interuniversitario di Ricerca della Chimica dei Metalli nei Sistemi Biologici (CIRC MSB) for support.

Funding statement. The research leading to these results has received funding from the European Research Council under the European Union's Seventh Framework Programme (FP7/2007-2013)/ERC grant agreement no. (249930-CoralWarm: Corals and global warming: the Mediterranean versus the Red Sea).

References

1. Spalding MD, Ravilious C, Green EP. 2001 *World atlas of coral reefs*. Berkeley, CA: University California Press.
2. Cohen AL, McConnaughey TA. 2003 Geochemical perspectives on coral mineralization. In *Biomineralization: reviews in mineralogy and geochemistry* (eds PM Dove, S Weiner, JJ Yoreo), pp. 151–187. Chantilly, VA: Mineralogical Society of America.
3. Marshall AT, Clode P. 2004 Calcification rate and the effect of temperature in a zooxanthellate and an azooxanthellate scleractinian reef coral. *Coral Reefs* **23**, 218–224. (doi:10.1007/s00338-004-0369-y)
4. Wilfert M, Peters W. 1969 Vorkommen von Chitin bei Couelenteraten. *Z. Morph. Tiere* **6**, 77–84. (doi:10.1007/BF00300386)
5. Cuif J-P, Dauphin Y, Berthet P, Jegoudez J. 2004 Associated water and organic compounds in coral skeletons: quantitative thermogravimetry coupled to infrared absorption spectrometry. *Geochem. Geophys. Geosyst.* **5**, Q11011.
6. Moberg F, Folke C. 1999 Ecological goods and services of coral reef ecosystems. *Ecol. Econ.* **29**, 215–233. (doi:10.1016/S0921-8009(99)00009-9)
7. Tambutté S, Holcomb M, Ferrier-Pages C, Reynaud S, Tambutté E, Zoccola D, Allemand D. 2011 Coral biomineralization: from the gene to the environment. *J. Exp. Mar. Biol. Ecol.* **408**, 58–78. (doi:10.1016/j.jembe.2011.07.026)
8. Constantz BR. 1986 Coral skeleton construction; a physiochemically dominated process. *Palaios* **1**, 52–157. (doi:10.2307/3514508)
9. Cuif J-P, Lecointre G, Perrin C, Tillier A, Tillier S. 2003 Patterns of septal biomineralization in scleractinian compared with their 28S rRNA phylogeny: a dual approach for a new taxonomic framework. *Zool. Scr.* **32**, 459–473. (doi:10.1046/j.1463-6409.2003.00133.x)
10. Cuif J-P, Dauphin Y, Doucet J, Salomé M, Susini J. 2003 XANES mapping of organic sulfate in three scleractinian coral skeletons. *Geochim. Cosmochim. Acta* **76**, 75–83. (doi:10.1016/S0016-7037(02) 01041-4)
11. Chamberlain JA. 1978 Mechanical properties of coral skeleton: compressive strength and its adaptive significance. *Paleobiology* **4**, 419–435.
12. Guillemin G, Patat JL, Fournie J, Chetail M. 1987 The use of coral as a bone graft substitute. *J. Biomed. Mater. Res.* **21**, 557–567. (doi:10.1002/jbm.820210503)
13. Li X, Chang WC, Chao YJ, Wang R, Chang M. 2004 Nanoscale structural and mechanical characterization of a natural nanocomposite material: the shell of red abalone. *Nano Letters* **4**, 613–617. (doi:10.1021/nl049962k)
14. Presser V, Gerlach K, Vohrer A, Nickel KG, Dreher WF. 2010 Determination of the elastic modulus of highly porous samples by nanoindentation: a case study on sea urchin spines. *J. Mater. Sci.* **45**, 2408–2418. (doi:10.1007/s10853-010-4208-y)
15. Kunitake ME, Mangano LM, Peloquin JM, Baker SP, Estroff LA. 2013 Evaluation of strengthening mechanisms in calcite single crystals from mollusk shells. *Acta Biomater.* **9**, 5353–5359. (doi:10.1016/j.actbio.2012.09.030)
16. Fleischli FD, Dietiker M, Borgia C, Spolenak R. 2008 The influence of internal length scales on mechanical properties in natural nanocomposites: a comparative study on inner layers of seashells. *Acta Biomater.* **4**, 1694–1706. (doi:10.1016/j.actbio.2008.05.029)
17. Stempflé PH, Pantalé O, Rousseau M, Lopez E, Bourrat X. 2010 Mechanical properties of the elemental nanocomponents of nacre structure. *Mater. Sci. Eng. C* **30**, 715–721. (doi:10.1016/j.msec.2010.03.003)
18. Wu YC, Lee TM, Chiu KH, Shaw SY, Yang CY. 2009 A comparative study of the physical and mechanical properties of three natural corals based on the criteria for bone–tissue engineering scaffolds. *J. Mater. Sci. Mater. Med.* **20**, 1273–1280. (doi:10.1007/s10856-009-3695-3)
19. Goldstein SA. 1987 The mechanical properties of trabecular bone: dependence on anatomic location and function. *J. Biomech.* **20**, 1055–1061. (doi:10.1016/0021-9290(87)90023-6)
20. Gong YUT, Killian CE, Olson IC, Appathurai NP, Amasino AL, Martin MC, Holt LJ, Wilt FH. 2012 Phase transitions in biogenic amorphous calcium carbonate. *Proc. Natl Acad. Sci. USA* **109**, 6088–6093. (doi:10.1073/pnas.1118085109)
21. Oliver WC, Pharr GM. 2004 Measurement of hardness and elastic modulus by instrumented indentation: advances in understanding and refinements to methodology. *J. Mater. Res.* **19**, 3–20. (doi:10.1557/jmr.2004.19.1.3)
22. Bull SJ. 2005 Nanoindentation of coatings. *J. Phys. D, Appl. Phys.* **38**, R393–R413. (doi:10.1088/0022-3727/38/24/R01)
23. Han YH, Li H, Wong TY, Bradt RC. 1991 Knoop microhardness anisotropy of single-crystal aragonite. *J. Am. Ceram. Soc.* **74**, 3129–3132. (doi:10.1111/j.1151-2916.1991.tb04311.x)
24. Kearney C, Zhao Z, Bruet BJF, Radovitzky R, Boyce MC, Ortiz C. 2006 Nanoscale anisotropic plastic deformation in single crystal aragonite. *Phys. Rev. Lett.* **96**, 255505. (doi:10.1103/PhysRevLett.96.255505)
25. Nowick AS. 1995 *Crystal properties via group theory*. Cambridge, UK: Cambridge University Press.
26. Liu L, Chen C, Lin C, Yang Y. 2005 Elasticity of single-crystal aragonite by Brillouin spectroscopy. *Phys. Chem. Minerals* **32**, 97–102. (doi:10.1007/s00269-005-0454-y)
27. Ungureanu CG, Prencipe M, Cossio R. 2010 Ab initio quantum-mechanical calculation of $CaCO_3$ aragonite at high pressure: thermodynamic properties and comparison with experimental data. *Eur. J. Miner.* **22**, 693–701. (doi:10.1127/0935-1221/2010/0022-2054)
28. Fantazzini P *et al*. 2013 A time-domain nuclear magnetic resonance study of Mediterranean scleractinian corals reveals skeletal-porosity sensitivity to environmental changes. *Environ. Sci. Technol.* **47**, 12 679–12 686. (doi:10.1021/es402521b)
29. Falini G, Reggi M, Fermani S, Sparla F, Goffredo S, Dubinsky Z, Levy O, Dauphin Y, Cuif JP. 2013 Control of aragonite deposition in colonial corals by intra-skeletal macromolecules. *J. Struct. Biol.* **183**, 226–238. (doi:10.1016/j.jsb.2013.05.001)
30. Stambler N, Dubinsky Z. 2005 Corals as light collectors: an integrating sphere approach. *Coral Reefs* **24**, 1–9. (doi:10.1007/s00338-004-0452-4)
31. Kaandorp JA, Sloot PMA. 2001 Morphological models of radiate accretive growth and the influence of hydrodynamics. *J. Theor. Biol.* **209**, 257–274. (doi:10.1006/jtbi.2001.2261)
32. Meroz E, Brickner I, Loya Y, Peretzman-Shemer A, Ilan M. 2002 The effect of gravity on coral morphology. *Proc. R. Soc. Lond. B* **269**, 717–720. (doi:10.1098/rspb.2001.1924)
33. Weiner S, Wagner HD. 1998 The material bone: structure–mechanical function relations. *Annu. Rev. Mater. Res.* **28**, 271–298. (doi:10.1146/annurev.matsci.28.1.271)
34. Fratzl P. 2008 Bone fracture: when the cracks begin to show. *Nature Mater.* **7**, 610–612. (doi:10.1038/nmat2240)
35. Seto J, Gupta HS, Zaslansky P, Wagner HD, Fratzl P. 2008 Tough lessons from bone: extreme mechanical anisotropy at the mesoscale. *Adv. Funct. Mater.* **18**, 1905–1911. (doi:10.1002/adfm.200800214)
36. Wang R, Gupta HS. 2011 Deformation and fracture mechanisms of bone and nacre. *Annu. Rev. Mater. Res.* **41**, 41–73. (doi:10.1146/annurev-matsci-062910-095806)
37. Hobatho MC, Rho JY, Ashman RB. 1997 Anatomical variation of human cancellous bone mechanical properties *in vitro*. *Stud. Health Technol. Inf.* **40**, 157–173.